ELSEVIER

Journal of Fluids and Structures 24 (2008) 1021–1041

JOURNAL OF FLUIDS AND STRUCTURES

www.elsevier.com/locate/jfs

Coupled hydrodynamic and structural analysis of compressible jet impact onto elastic panels

A.A. Korobkin[a], T.I. Khabakhpasheva[a,*], G.X. Wu[b]

[a]*Lavrentyev Institute of Hydrodynamics, SB RAS, 630090 Novosibirsk, Russia*
[b]*Department of Mechanical Engineering, University College London, Torrington Palace, London WC1E 7JE, UK*

Received 14 December 2006; accepted 4 March 2008
Available online 22 August 2008

Abstract

This paper is concerned with the initial stage of a compressible liquid jet impact onto an elastic plate. The fluid flow is governed by the linear wave equation, while the response of the plate is governed by the classical linear dynamical plate equation. The coupling between the fluid flow and the plate deflection is taken into account through the dynamic and kinematic conditions imposed on the wetted part of the plate. The problem is solved numerically by the normal mode method. The principal coordinates of the hydrodynamic pressure and plate deflections satisfy a system of ordinary differential and integral equations. A time stepping method based on the Runge–Kutta scheme is used for the numerical integration of the system. Calculations are performed for two-dimensional, axisymmetric and three-dimensional jet impacts onto an elastic plate. The effects of the impact conditions and the elastic properties of the plate on the magnitudes of the elastic deflections and bending stresses are analysed.

Keywords: Compressible liquid jet impact; Elastic plate; Normal mode method; Deflection; Bending stresses

1. Introduction

The problem of liquid impact onto an elastic panel is of importance in many engineering applications. Sloshing in a liquefied natural gas (LNG) tank [see, for example, Bredmose et al. (2002)] can be very violent and the liquid cargo can hit the tank walls and its ceiling with a strong force in the form of jet. In extreme cases, the wall or the ceiling can be damaged and LNG leakage may occur. Another example is an offshore platform in rough seas where the interaction of steep surface waves with the legs of the platform may lead to the development of a jet, which travels up the platform leg with high speed and hits the lower deck of the platform from below. Such impacts may damage the lower surface of the platform. Jet impact may also occur through slamming and "water-on-deck" phenomena when a ship is in a severe sea environment. In the former case the ship bow emerges from the water and then plunges into the water at high speed producing splashing jets as a result. In the latter case, water comes onto the ship and travels over the deck impacting obstacles in its path. Other examples include steep waves or tsunami impact on offshore and coastal structures. There are many cases where loss of life and damage has been caused by these kind of impact forces. Research into jet impact

*Corresponding author. Tel.: +7 383 333 30 66; fax: +7 383 333 16 12.
E-mail address: tana@hydro.nsc.ru (T.I. Khabakhpasheva).

0889-9746/$ - see front matter © 2008 Elsevier Ltd. All rights reserved.
doi:10.1016/j.jfluidstructs.2008.03.002

onto elastic structures is therefore of great practical importance. An appropriate approach to this problem is a coupled hydrodynamic and structural analysis.

Flexibility of the structure is very important in fluid–structure interaction. If the jet speed is very high, the structure can be broken. For moderate impact velocities the structure can be damaged with the formation of cracks and change of the structure shape. Low-speed jets may bring no immediate visible damage, but repeated impacts over time can lead to fatigue damage of the structure surface.

For fatigue analysis we should estimate the value of the maximal stresses in the structure and identify the locations where these maximal stresses occur. Estimates should be obtained in terms of the impact conditions, which include the physical properties and geometrical characteristics of the structure, and the speed and shape of the jet.

This work considers the very early stage of jet impact on a flexible panel. Because of the rapid temporal variation, acoustic effects will be important in the liquid. In other words, the compressibility of the liquid should be taken into account within the time scale inversely proportional to the speed of the sound in the liquid. Through the integration of the dynamic and kinematic conditions on the jet surface with respect to time, one can then adopt the approximation that the free surface remains unchanged and the velocity remains zero on the undisturbed surface during this short period.

The deformation of the panel is modelled by the linear dynamical plate equation. The coupling between the fluid flow and deflection of the panel is achieved through the dynamic and kinematic conditions on the wetted surface of the panel. There are two time scales in this coupled problem. The first one is related to the impact within which compressible effects are important. The second one is related to deflection of the plate and can be measured by the first natural period of plate oscillation. Strictly speaking, these two time scales should be comparable for the model to be used. In reality, the second time scale is usually much larger than the first one. The time-marching based method in this paper has been carried out well beyond the first period of the plate, or the second time scale, with the time step much smaller than the first time scale. Even though the linear compressible model may not be fully applicable in the second time scale, the simulations carried out could provide some insight into the acoustic effect on the solution of the coupled problem. The high frequency modes of the plate have natural periods which may be comparable to the acoustic scale. The present procedure is then fully consistent. Moreover, if the liquid is aerated in the impact region, then the sound speed in the air/liquid mixture could be as low as 20 m/s (Wu, 1991) and the acoustic time scale could be comparable to the first natural period of plate oscillation.

Strictly speaking, if the interest in impact is over a longer period, or when the simulation has to be carried out beyond the first time scale, the free surface deformation and potential variation along the free surface with time have to be taken into account. Lu et al. (2000) considered the water entry problem of an elastic wedge. They used an incompressible model and imposed fully nonlinear boundary conditions on the instantaneous position of the free surface. However, the present work focuses on the initial stage and the compressibility effect.

The present problem is dynamically equivalent to that of a plate moving suddenly into a stationary jet. This corresponds to an infinitely large initial acceleration. The acoustic effect will be much less pronounced if the plate moves into the jet with a finite acceleration. This case was investigated by King and Needham (1994) for a rigid vertical plate. They considered the initial stage of the flow and focused on an inner solution close to the intersection point between the plate and the free surface. The analysis provided the shape of the jet and its length in the leading order as time tends to zero. The free-surface deformation and the flow field caused by the impulsive horizontal motion of a rigid vertical plate into a horizontal strip of inviscid incompressible fluid, initially at rest, was studied by Needham et al. (2007) in the small time limit using the method of matched asymptotic expansions. The second-order velocity potential has been obtained in the "outer" region, the dimension of which is of the order of the liquid depth. This solution is singular at the point where the free surface meets the rigid wall. In polar coordinates (r, θ) with the center at the intersection point, the first-order velocity potential is of the order of $\mathcal{O}(r \log r)$ and the second-order potential of the order of $\mathcal{O}(\log^2 r)$ as $r \to 0$. Needham et al. (2007) derived and studied the inner solution with the aim of resolving these singularities. Note that within the linear theory both the velocity potential and the hydrodynamic pressure tend to zero as $r \to 0$ but their first derivatives with respect to the radial coordinate are singular at the intersection point. The present paper is concerned with the global effect of a jet impact on the deflection and stress of the plate within the linear theory.

The present analysis is similar to the work of Korobkin (1996), who treated the plate as rigid. He used the eigenfunctions for the jet cross-section and reduced the problem to a set of differential equations along the jet. The extension of this analysis to a flexible plate is not trivial. While the eigenfunctions for the fluid flow correspond to the shape of the jet cross-section, the eigenfunctions for the structural analysis correspond to the plate shape. These two sets of eigenfunctions are not orthogonal to each other. As a result, far more eigenfunctions are needed and the memory effect term involves far more complex integrands than in the case of jet impact onto a rigid plate.

In problems of hydroelasticity, the plate deflection and distribution of stresses in the plate are of primary importance for practical needs. However, the hydrodynamic loads and pressure distributions are still needed by designers. For this

reason, even though the deflection and stress in the plate can be obtained without direct calculations of the pressure, the results for pressure distributions are still provided.

In Section 2 the mathematical formulation of the coupled problem of impact and scaling is given. In Section 3 the hydrodynamic problem is analysed with the help of a modal approach and integral transforms. Section 4 contains a structural analysis of the problem by the normal mode method. The numerical procedure for solving the coupled problem is described in Section 5. Numerical results for two-dimensional jet impact onto a beam, three-dimensional jet impact onto rectangular and circular plates are presented in Sections 6, 7 and 8, respectively. The effects of impact conditions on the elastic response of the plate are analysed in each of these three sections. The main results of the study are outlined in Section 9.

2. Formulation of the problem

We consider a coupled problem of jet-structure impact. The structure is a single plate of uniform thickness. Its edges are simply supported or clamped. The jet hits the plate from below in the normal direction. Gravity and surface tension effects are neglected. The presence of air and, in particular, the air-cushion effect are not taken into account. The liquid is assumed ideal and weakly compressible. The front part of the jet is flat (see Fig. 1). Perturbations of the jet flow due to the impact are described within the acoustic approximation (Korobkin, 1996). This approach is applicable if the jet speed V is much smaller than the sound speed in the liquid c_0, that is, for low Mach number $M = V/c_0$. Experiments [see Eroshin et al. (1980)] indicate that the linear acoustic approximation can be used for analysis of water impact in the range of impact speeds $5\,\mathrm{m/s} < V < 100\,\mathrm{m/s}$.

We consider the initial stage of the impact, when the flow characteristics change rapidly with time. This stage, which is referred to below as the impact stage, is of short duration. This makes it possible to neglect deformations of the jet free surface, linearize the boundary conditions and impose them on the initial surface of the jet.

The problem is considered in nondimensional variables, where the characteristic dimension R of the jet cross-section D is the length scale, jet speed V is the velocity scale, the "water hammer" pressure $\rho c_0 V$ is the pressure scale, ρ is the liquid density, the product VR is the scale of the velocity potential of the flow in the jet region $(x, y) \in D$, $z < 0$ and RV/c_0 is the plate deflection scale, $Oxyz$ is the Cartesian coordinate system with the plate being in the plane $z = 0$ (see Fig. 1). The ratio R/c_0 is taken as the time scale.

In the nondimensional variables the liquid flow after the impact instant, $t = 0$, is described by the total velocity potential $z - \varphi(x, y, z, t)$, where φ is the disturbed potential which satisfies the following equations and boundary conditions:

$$\varphi_{tt} = \Delta\varphi \quad ((x, y) \in D, z < 0), \tag{1}$$

$$\varphi = 0 \quad ((x, y) \in \partial D, z < 0), \quad \varphi \to 0 \quad ((x, y) \in D, z \to -\infty), \tag{2}$$

$$\varphi_z = 1 - w_t(x, y, t) \quad ((x, y) \in D, z = 0), \tag{3}$$

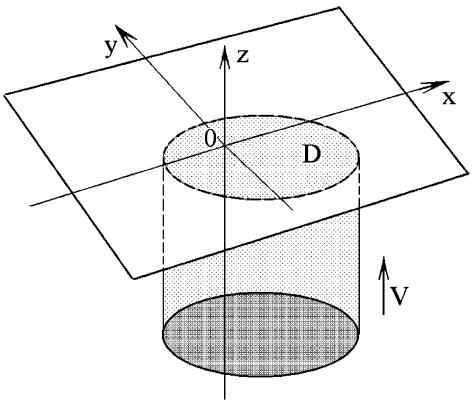

Fig. 1. Sketch of the jet–plate impact problem.

$$\varphi = \varphi_t = 0 \quad (t = 0), \tag{4}$$

$$p = \varphi_t, \tag{5}$$

where Δ is the Laplace operator, $w(x, y, t)$ is the plate deflection, $p(x, y, z, t)$ is the hydrodynamic pressure and ∂D is the boundary of the jet cross-section D. In the case of a rigid plate, $w = 0$; this problem was studied by Korobkin (1996).

The plate deflection is governed by the equation

$$\alpha w_{tt} + \beta \Delta^2 w = p(x, y, 0, t) \quad ((x, y) \in S, t > 0), \tag{6}$$

$$w = w_t = 0 \quad (t = 0), \tag{7}$$

where

$$\alpha = \frac{m}{\rho R}, \quad \beta = \frac{D_p}{\rho c_0^2 R^3},$$

$m = \rho_p h$ is the plate mass per unit area, ρ_p is the density of the plate material and h is the plate thickness, $D_p = Eh^3/[12(1 - \nu^2)]$ is the plate stiffness, E is Young's modulus, ν is the Poisson ratio and S is the surface area of the plate.

Boundary conditions for Eq. (6) are not specified at this stage and will be given for each specific problem. It can be seen that the problems under consideration (1)–(5) and (6)–(7) are coupled. The liquid flow and the plate deflection have to be determined simultaneously, which is a feature of hydroelasticity problems.

The coupled problem (1)–(7) is solved by the normal mode method, which is applied to both the hydrodynamic problem (1)–(5) and the structural problem (6)–(7). The method is designed in such a way that it can deal with a jet of an arbitrary cross-section and elastic plate of an arbitrary shape.

3. Hydrodynamic analysis

The velocity potential $\varphi(x, y, z, t)$ is sought in the form

$$\varphi(x, y, z, t) = \sum_{k=1}^{\infty} M_k(t, z) A_k(x, y), \tag{8}$$

where $A_k(x, y)$ are eigenfunctions satisfying equations

$$\frac{\partial^2 A_k}{\partial x^2} + \frac{\partial^2 A_k}{\partial y^2} + \lambda_k^2 A_k = 0 \quad ((x, y) \in D), \tag{9}$$

$$A_k = 0 \quad ((x, y) \in \partial D)$$

and the orthogonality condition

$$\int_D A_k(x, y) A_n(x, y)\, \mathrm{d}x\, \mathrm{d}y = \delta_{n,k}, \tag{10}$$

where λ_k are the eigenvalues, $\delta_{n,k} = 0$ for $n \neq k$ and $\delta_{n,n} = 1$.

From Eqs. (1)–(4) it follows that the unknown functions $M_k(t, z)$ should satisfy the equation

$$\frac{\partial^2 M_k}{\partial t^2} = \frac{\partial^2 M_k}{\partial z^2} - \lambda_k^2 M_k \quad (z < 0, t > 0), \tag{11}$$

the initial conditions

$$M_k = \frac{\partial M_k}{\partial t} = 0 \quad (z < 0, t = 0), \tag{12}$$

the boundary condition

$$\frac{\partial M_k}{\partial z}(t, 0) = c_k - \frac{\mathrm{d}}{\mathrm{d}t} \Upsilon_k(t), \tag{13}$$

$$c_k = \int_D A_k(x, y)\, \mathrm{d}x\, \mathrm{d}y, \quad \Upsilon_k(t) = \int_D w(x, y, t) A_k(x, y)\, \mathrm{d}x\, \mathrm{d}y \tag{14}$$

and the far-field condition

$$M_k(t,z) \to 0 \quad (z \to -\infty). \tag{15}$$

Once the functions $M_k(t,z)$ have been evaluated, the pressure in the impact region, $(x,y) \in D, z = 0$, can be obtained as

$$p(x,y,0,t) = \sum_{k=1}^{\infty} \frac{\partial M_k}{\partial t}(t,0) A_k(x,y). \tag{16}$$

We apply the Laplace transform to Eqs. (11)–(15). This gives

$$\begin{aligned} &(s^2 + \lambda_k^2) M_k^L = \frac{\partial^2 M_k^L}{\partial z^2} \quad (z<0), \\ &\frac{\partial M_k^L}{\partial z} = \frac{c_k}{s} - s\Upsilon_k^L \quad (z=0), \\ &M_k^L \to 0 \quad (z \to -\infty), \end{aligned} \tag{17}$$

where superscript L indicates Laplace transform. From the solution of $M_k^L(s,z)$ we obtain

$$\left[\frac{\partial M_k}{\partial t}\right]^L (s,0) = sM_k^L = \frac{c_k}{\sqrt{s^2+\lambda_k^2}} - s^2 \frac{\Upsilon_k^L}{\sqrt{s^2+\lambda_k^2}}. \tag{18}$$

The inverse Laplace transform then leads to

$$\frac{\partial M_k}{\partial t}(t,0) = c_k \mathrm{J}_0(\lambda_k t) - \frac{\mathrm{d}^2}{\mathrm{d}t^2} \int_0^t \Upsilon_k(\tau) \mathrm{J}_0[\lambda_k(t-\tau)]\,\mathrm{d}\tau. \tag{19}$$

Here $\mathrm{J}_0(x)$ is the Bessel function of zero order. From Eqs. (16) and (19) the pressure distribution in the contact region can be found as

$$p(x,y,0,t) = \sum_{k=1}^{\infty} c_k A_k(x,y) \mathrm{J}_0(\lambda_k t) - \frac{\partial^2}{\partial t^2} \sum_{k=1}^{\infty} A_k(x,y) \int_0^t \Upsilon_k(t) \mathrm{J}_0[\lambda_k(t-\tau)]\,\mathrm{d}\tau. \tag{20}$$

The first term on the right-hand side of Eq. (20) is the pressure caused by compressible jet impact onto a rigid plate and the second term corresponds to the convolution effect of the plate flexibility, or the "memory effect".

For a rigid plate and incompressible liquid the tangential velocity at the intersection point is found to be singular (Peregrine, 1972). The nature of this singularity within the framework of a flexible plate and compressible liquid is not pursued here, as the dynamic coupling between the plate and the liquid is through the pressure. The pressure at the intersection can be discontinuous for a rigid plate and incompressible liquid (Wu, 2001). Whether this discontinuity remains in the present problem becomes less obvious, as shown in Eq. (20). In any case, the possible discontinuity will not affect the global results of deflection and stress, as it occurs only at the intersection points. This can be confirmed in the numerical simulation through using more terms in the expansion in the convergence study.

4. Structural analysis

The structural part of the problem is solved with the help of the normal mode method. This method was successfully used in the two-dimensional problem of beam-liquid impact (Korobkin, 1998; Korobkin and Khabakhpasheva, 2006). The plate deflection is sought in the form

$$w(x,y,t) = \sum_{m=1}^{\infty} a_m(t) \psi_m(x,y), \tag{21}$$

where the functions $\psi_m(x,y)$ are non-trivial solutions of the homogeneous problem

$$\Delta^2 \psi_m = \kappa_m^4 \psi_m \quad ((x,y) \in S) \tag{22}$$

and κ_m are the corresponding eigenvalues. Appropriate boundary conditions are imposed on ∂S, which are the same as for the plate under consideration. The eigenfunctions $\psi_m(x,y)$ satisfy the orthogonality condition

$$\int_S \psi_m(x,y) \psi_n(x,y)\,\mathrm{d}x\,\mathrm{d}y = \delta_{m,n}. \tag{23}$$

By substituting Eq. (21) into Eq. (6), multiplying the result by $\psi_n(x,y)$ and integrating over the plate area S, we arrive at the equations with respect to the principal coordinates $a_n(t)$:

$$\alpha\ddot{a}_n + \beta\kappa_n^4 a_n = \int_D p(x,y,0,t)\psi_n(x,y)\,\mathrm{d}x\,\mathrm{d}y. \tag{24}$$

Note that in this equation the integral is over the contact region D but not over the plate area S since $p \equiv 0$ outside of the contact region.

Eq. (21) makes it possible to write the functions $\Upsilon_k(t)$ from Eq. (14) as

$$\Upsilon_k(t) = \sum_{m=1}^{\infty} a_m(t) T_{km},$$

where

$$T_{km} = \int_D A_k(x,y)\psi_m(x,y)\,\mathrm{d}x\,\mathrm{d}y. \tag{25}$$

Using Eq. (20) we obtain

$$\int_D p(x,y,0,t)\psi_n(x,y)\,\mathrm{d}x\,\mathrm{d}y = \sum_{k=1}^{\infty} c_k T_{kn} \mathrm{J}_0(\lambda_k t) - \frac{\mathrm{d}^2}{\mathrm{d}t^2}\sum_{k=1}^{\infty} T_{kn}\int_0^t \Upsilon_k(\tau)\mathrm{J}_0[\lambda_k(t-\tau)]\,\mathrm{d}\tau. \tag{26}$$

Eqs. (24) and (26) are combined to give

$$\frac{\partial^2}{\partial t^2}\left\{\alpha a_n + \sum_{k=1}^{\infty} T_{kn}\int_0^t \Upsilon_k(\tau)\mathrm{J}_0[\lambda_k(t-\tau)]\,\mathrm{d}\tau\right\} + \beta\kappa_n^4 a_n = q_n(t),$$

where

$$q_n(t) = \sum_{k=1}^{\infty} c_k T_{kn}\mathrm{J}_0(\lambda_k t), \tag{27}$$

$$\sum_{k=1}^{\infty} T_{kn}\int_0^t \Upsilon_k(\tau)\mathrm{J}_0[\lambda_k(t-\tau)]\,\mathrm{d}\tau = \sum_{m=1}^{\infty}\int_0^t a_m(\tau)\left\{\sum_{k=1}^{\infty} T_{kn}T_{km}\mathrm{J}_0[\lambda_k(t-\tau)]\right\}\mathrm{d}\tau.$$

It is convenient to introduce the functions

$$K_{nm}(t) = \sum_{k=1}^{\infty} T_{kn}T_{km}\mathrm{J}_0(\lambda_k t), \quad K_{nm}(t) = K_{mn}(t) \tag{28}$$

and the new unknown functions $b_n(t)$ and $r_n(t)$

$$b_n(t) = \alpha a_n + \sum_{m=1}^{\infty}\int_0^t a_m(\tau)K_{nm}(t-\tau)\,\mathrm{d}\tau,$$

$$\frac{\mathrm{d}b_n}{\mathrm{d}t} = r_n(t).$$

With these definitions, the plate equation is reduced to

$$\frac{\mathrm{d}r_n}{\mathrm{d}t} = q_n - \beta\kappa_n^4 a_n.$$

Finally, we obtain a system of ordinary differential equations in vector form

$$\frac{\mathrm{d}\vec{b}}{\mathrm{d}t} = \vec{r}, \tag{29}$$

$$\frac{\mathrm{d}\vec{r}}{\mathrm{d}t} = \vec{q} - \beta\mathbf{D}\vec{a} \tag{30}$$

and a system of integral equations

$$\alpha\vec{a}(t)+\int_0^t \mathbf{K}(t-\tau)\vec{a}(\tau)\,\mathrm{d}\tau=\vec{b}(t), \tag{31}$$

subject to the initial conditions

$$\vec{b}(0)=0,\quad \vec{a}(0)=0,\quad \vec{r}(0)=0, \tag{32}$$

where

$$\vec{q}(t)=[q_1(t),q_2(t),\dots]^{\mathrm{T}},\quad \vec{b}(t)=[b_1(t),b_2(t),\dots]^{\mathrm{T}},$$

$$\vec{a}(t)=[a_1(t),a_2(t),\dots]^{\mathrm{T}},\quad \vec{r}(t)=[r_1(t),r_2(t),\dots]^{\mathrm{T}},$$

$\mathbf{K}(t)$ is symmetric matrix with elements $K_{nm}(t)$ and $\mathbf{D}=\mathrm{diag}\{\kappa_1^4,\kappa_2^4,\dots\}$ is a diagonal matrix.

5. Numerical procedure

To solve the jet impact problem numerically, we first determine the eigenfunctions $A_k(x,y)$, $\psi_m(x,y)$ from Eqs. (9) and (22), and the corresponding eigenvalues λ_k and κ_m for $k\leqslant N_j, m\leqslant N_p$. These functions are arranged in such a way that $\lambda_{k+1}\geqslant\lambda_k$ and $\kappa_{m+1}\geqslant\kappa_m$. Then we evaluate the quantities c_k, T_{km} by Eqs. (14) and (25) and the functions $q_n(t)$, $K_{nm}(t)$, by Eqs. (27) and (28), where $n\leqslant N_p$, $m\leqslant n$ and $t\geqslant 0$.

The integral in Eq. (31) is subdivided into two integrals along the intervals $[0,t-\frac{1}{2}\Delta t]$ and $[t-\frac{1}{2}\Delta t,t]$. The first integral is evaluated by the trapezoidal rule with the integration step equal to $\frac{1}{2}\Delta t$. The integral over the interval $[t-\frac{1}{2}\Delta,t]$ is computed by using quadratic approximation of the integrand on the interval $[t-\Delta t,t]$:

$$\alpha\vec{a}(t)+\frac{5\Delta t}{24}\mathbf{K}(0)\vec{a}(t)=\vec{b}(t)-\int_0^{t-\Delta t/2}\mathbf{K}(t-\tau)\vec{a}(\tau)\,\mathrm{d}\tau+\frac{\Delta t}{24}\mathbf{K}(\Delta t)\vec{a}(t-\Delta t)-\frac{\Delta t}{3}\mathbf{K}\left(\frac{1}{2}\Delta t\right)\vec{a}\left(t-\frac{1}{2}\Delta t\right). \tag{33}$$

The time step Δt is chosen in such a way that the functions $q_n(t)$ and $K_{nm}(t)$ for each interval $(j\Delta t,(j+1)\Delta t)$ are accurately represented with the help of linear interpolation. The system of differential equations (29) and 30 is solved numerically by the fourth-order Runge–Kutta method. The values of $\vec{a}((\Delta t/2)j)$, $j\geqslant 1$, are calculated by using Eq. (33), where the forcing term $\vec{b}((\Delta t/2)j)$ comes from the solution of Eqs. (29) and (30). The integration of Eqs. (29)–(31) is performed with different steps Δt until convergence has been achieved.

Once the principal coordinates $a_n(t)$ have been obtained, one can evaluate the plate deflection and internal stresses. The pressure distribution over the contact region is computed with the help of the formula

$$p(x,y,0,t)=\sum_{k=1}^{\infty}p_k(t)A_k(x,y), \tag{34}$$

where

$$p_k(t)=c_k\mathrm{J}_0(\lambda_k t)-\sum_{m=1}^{\infty}T_{km}\left\{\dot{a}_m(t)+\lambda_k^2\int_0^t a_m(\tau)P_k(t-\tau)\,\mathrm{d}\tau\right\}, \tag{35}$$

$$P_k(t)=\frac{\mathrm{J}_1(\lambda_k t)}{\lambda_k t}-\mathrm{J}_0(\lambda_k t). \tag{36}$$

Here $\mathrm{J}_1(x)$ is the Bessel function of first order. For all calculations performed in this paper, a steel plate is chosen with $E=21\times10^{10}\,\mathrm{N/m^2}$, $\rho_p=7875\,\mathrm{kg/m^3}$, $\nu=0.3$. The water jet parameters are $c_0=1500\,\mathrm{m/s}$, $\rho=1000\,\mathrm{kg/m^3}$. In what follows, all dimensional quantities are indicated with a tilde.

6. Two-dimensional problem of jet impact

A sketch of a two-dimensional jet impact problem is shown in Fig. 2. The jet width $\tilde{a}_j$ is taken as the length scale R of the problem. In dimensionless variables, a_p is the plate length and c is the distance of the jet centre from the left end of the plate. The plate is modelled as a simply supported beam of constant thickness $\tilde{h}$. The hydrodynamic part of the

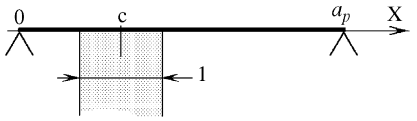

Fig. 2. Sketch of the two-dimensional impact problem.

original problem Eqs. (1)–(7) provides

$$\varphi_{tt} = \varphi_{xx} + \varphi_{zz} \quad (c - \tfrac{1}{2} < x < c + \tfrac{1}{2},\ z < 0),$$

$$\varphi = 0 \quad (x = c \pm \tfrac{1}{2},\ z < 0),$$

$$\varphi_z = 1 - w_t(x,t) \quad (c - \tfrac{1}{2} < x < c + \tfrac{1}{2},\ z = 0).$$

Eqs. (9) for the eigenfunctions of the jet cross-section take the forms

$$\frac{\partial^2 A_k}{\partial x^2} + \lambda_k^2 A_k = 0 \quad (c - \tfrac{1}{2} < x < c + \tfrac{1}{2}),$$

$$A_k = 0 \quad (x = c \pm \tfrac{1}{2}).$$

Non-trivial solutions of this homogeneous problem are

$$A_k(x) = \sqrt{2}\sin[\lambda_k(x - (c - \tfrac{1}{2}))], \quad \lambda_k = \pi k \ \ (k \geqslant 1).$$

Eq. (14) provides

$$c_k = \frac{\sqrt{2}}{\pi k}(1 - (-1)^k).$$

In the two-dimensional problem, the plate region S corresponds to the interval $(0, a_p)$ and Eq. (22) takes the form

$$\frac{\mathrm{d}^4 \psi_m}{\mathrm{d}x^4} = \kappa_m^4 \psi_m \quad (0 < x < a_p).$$

For a simply supported beam the boundary conditions are

$$\psi_m = 0, \quad \frac{\mathrm{d}^2 \psi_m}{\mathrm{d}x^2} = 0 \quad (x = 0 \text{ or } x = a_p).$$

We find

$$\psi_m(x) = \sqrt{\frac{2}{a_p}}\sin(\kappa_m x), \quad \kappa_m = \frac{\pi m}{a_p} \quad (m \geqslant 1).$$

Eq. (25) gives

$$T_{km} = \int_{c-1/2}^{c+1/2} A_k(x)\psi_m(x)\,\mathrm{d}x = \sqrt{\frac{1}{a_p}}\left\{\frac{\sin[\alpha_-(1)]}{\alpha_-(1)}\cos[\alpha_-(2c)] - \frac{\sin[\alpha_+(1)]}{\alpha_+(1)}\cos[\alpha_+(2c)]\right\},$$

where

$$\alpha_-(x) = \frac{\pi}{2}\left(k - x\frac{m}{a_p}\right), \quad \alpha_+(x) = \frac{\pi}{2}\left(k + x\frac{m}{a_p}\right).$$

In the numerical calculations the plate length $\tilde{a}_p$ varies from 50 cm to 4 m, the plate thickness $\tilde{h}$ from 0.5 to 5 cm and the jet width $\tilde{a}_j$ from 10 cm to 1 m. The calculations are performed in the nondimensional variables. The number of modes N_p for the plate deflection and N_j for the jet vary from 3 to 50. Numerical tests revealed that at least 10 modes must be used both for the structural and for hydrodynamic analysis. The time step Δt is in the range from 0.001 to 0.05. If the number of modes N_p or N_j increase, the time step must be reduced.

Results, depicted in Figs. 3–8 are obtained for the plate length $\tilde{a}_p = 1$ m, the plate thickness $\tilde{h} = 2$ cm and the jet width $\tilde{a}_j = 20$ cm. The distance from the left end of the plate to the jet centre is $\tilde{c} = 25$ cm. In nondimensional variables $a_p = 5$ and $c = 1.25$. The impact velocity is 25 m/s. Hydrodynamic pressure and plate deflection are linearly dependent

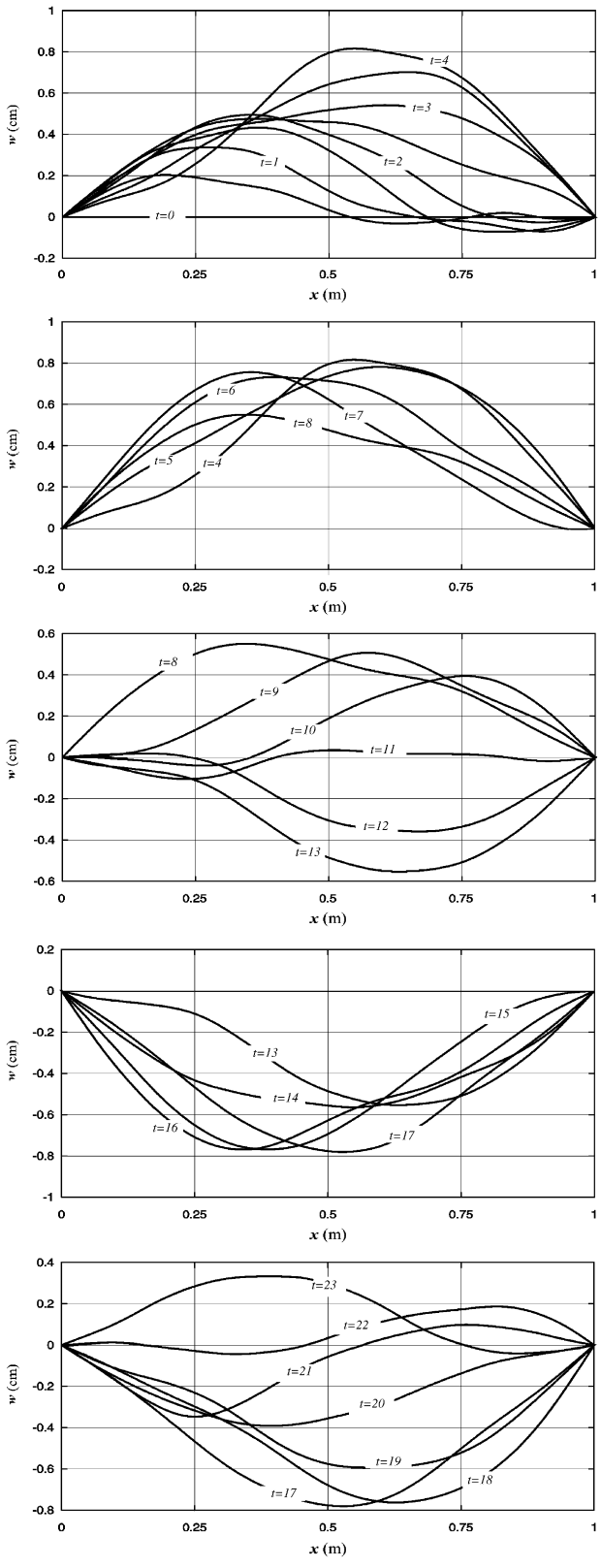

Fig. 3. Evolution of the plate deflection (time t is given in microseconds).

on the impact velocity. The number of modes are equal to 20 for the structural analysis (N_p) and 10 for the hydrodynamic analysis (N_j). The dimensionless time step is chosen as $\Delta t = 0.05$, which corresponds to 6.7×10^{-6} s in the dimensional variables.

Fig. 3 presents the evolution of the plate deflection (the unit of time is the microsecond). It can be seen that plate vibrates owing to the impact. The position of the maximal deflection moves along the plate during the impact. This implies that the contributions of the higher modes are important. A simplified approach with $N_p = 1$ is not expected to give appropriate estimates of maximal stresses caused by the jet impact.

Fig. 4 presents the time history of the plate deflections at the plate centre and at the jet centre, maximal and minimal deflections along the plate. It is important to note that the periods of free vibrations of the plate are given by the formulae [see Timoshenko (1955)]

$$T_n^{(f)} = \frac{2\pi}{\omega_n}, \quad \omega_n = \frac{\pi^2 n^2}{\tilde{a}_p^2}\sqrt{\frac{D_p}{\rho_p \tilde{h}}}.$$

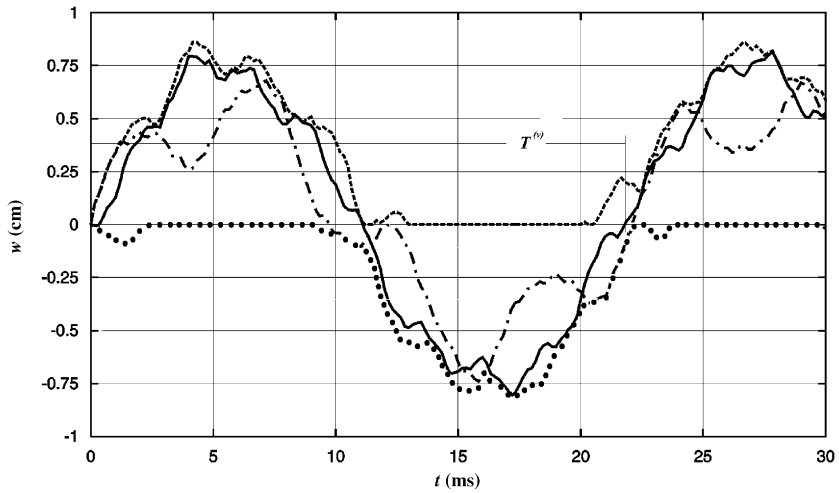

Fig. 4. Evolution of the plate deflections at the plate centre (solid line) and at the jet centre (chain-dotted line), maximal (dashed line) and minimal (dotted line) deflections along the plate at each time instant.

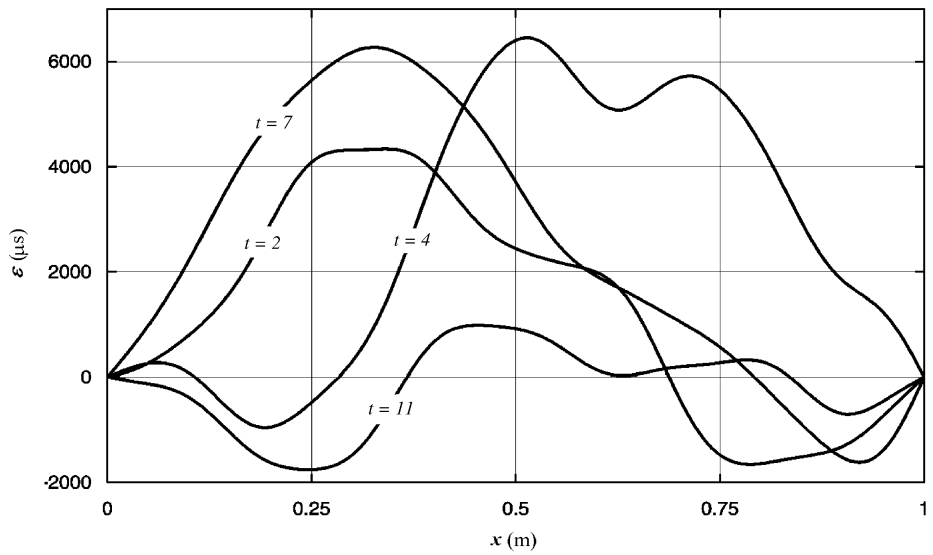

Fig. 5. Evolution of the strain distribution along the plate (time t is in microseconds).

For a steel plate with $\tilde{a}_p = 1\,\mathrm{m}$ and $\tilde{h} = 2\,\mathrm{cm}$ we obtain $T_1^{(f)} = 20.4\,\mathrm{ms}$, $T_2^{(f)} = 5.1\,\mathrm{ms}$ and $T_3^{(f)} = 2.26\,\mathrm{ms}$. The plate deflections in Fig. 4 are not entirely periodic, which is due to the memory effect. As a rough estimate of the main period $T^{(v)}$ of the plate vibration due to the impact, we use the time between the two zero points of the curves, which gives $T^{(v)} \approx 22\,\mathrm{ms}$. This is longer than the first mode period $T_1^{(f)}$ of free plate vibration, which is due to the added mass effect.

Evolution of the strain distribution along the plate is presented in Fig. 5 for $t = 2, 4, 7$ and 11 ms. These curves exhibit stronger oscillations than the deflection curves (see Figs. 3 and 4). At each time instant the strain distribution is smooth but the strain maximum changes very fast in time (see Fig. 6).

Figs. 7 and 8 present the evolution of the pressure at the jet centre (Fig. 7) and pressure distribution along the contact region (Fig. 8) in dimensionless variables. The thick line in Fig. 7 corresponds to $N_j = N_p = 30$ modes and the thin line corresponds to $N_j = N_p = 10$ modes. It can be seen that these two lines are in a fairly good agreement. Moreover, calculations were performed with $N_j = N_p = 50$ modes and the result was found to be very close to that for $N_j = N_p = 30$ modes.

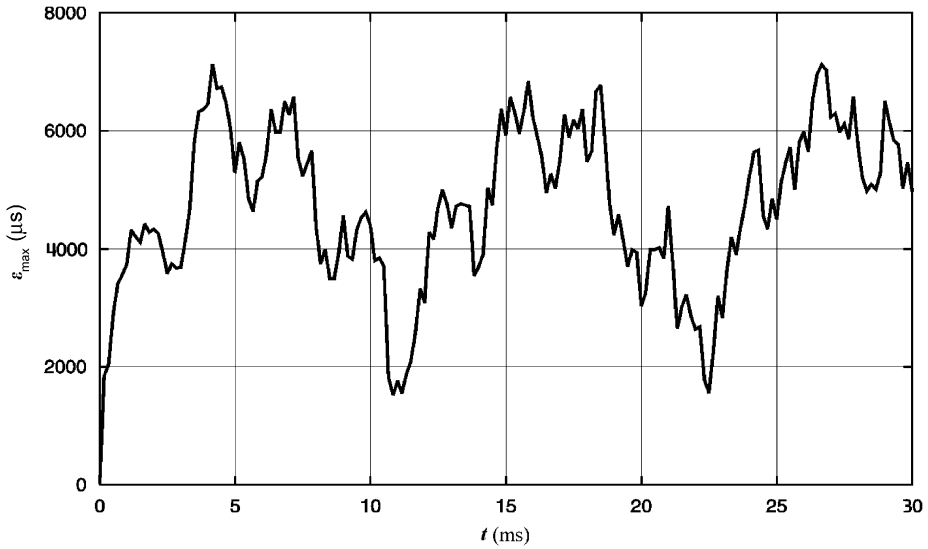

Fig. 6. Time history of maximal strain in the plate.

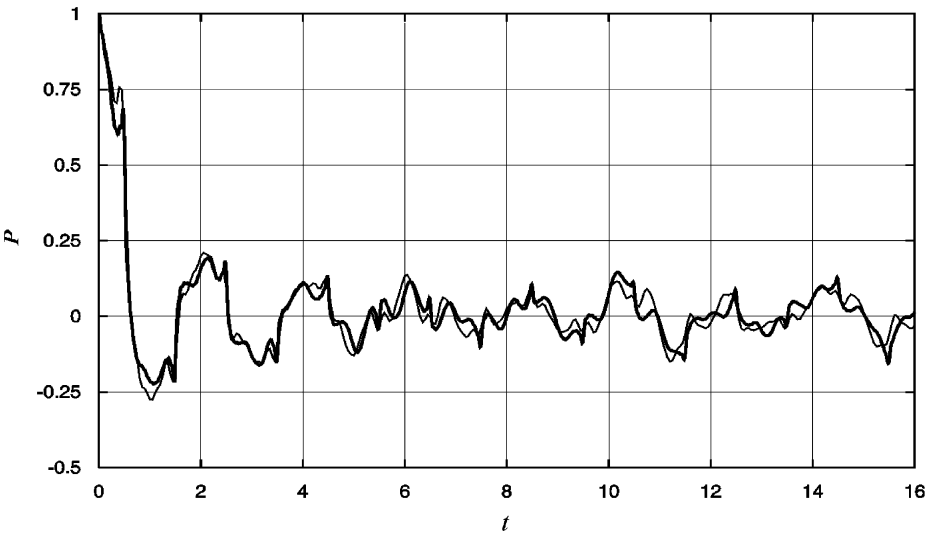

Fig. 7. Pressure at the centre of the jet in nondimensional form, calculated with different numbers of modes.

Fig. 7 demonstrates that the acoustic effects are most important during the very initial stage, duration of which can be roughly estimated as R/c_0 and in the nondimensional variables as $t<1$. Rapid temporal evolution of the pressure can be observed during this stage. The pressure decreases thereafter and oscillates around zero. This behaviour can be partly explained by the pressure wave propagated from the jet surface into the contact region [see Korobkin (1996) for details]. At each time instant the pressure distribution along the plate is smooth (see Fig. 8). Numerical simulations showed that the way the pressure distribution evolves in time does not strongly depend on the location of the impact.

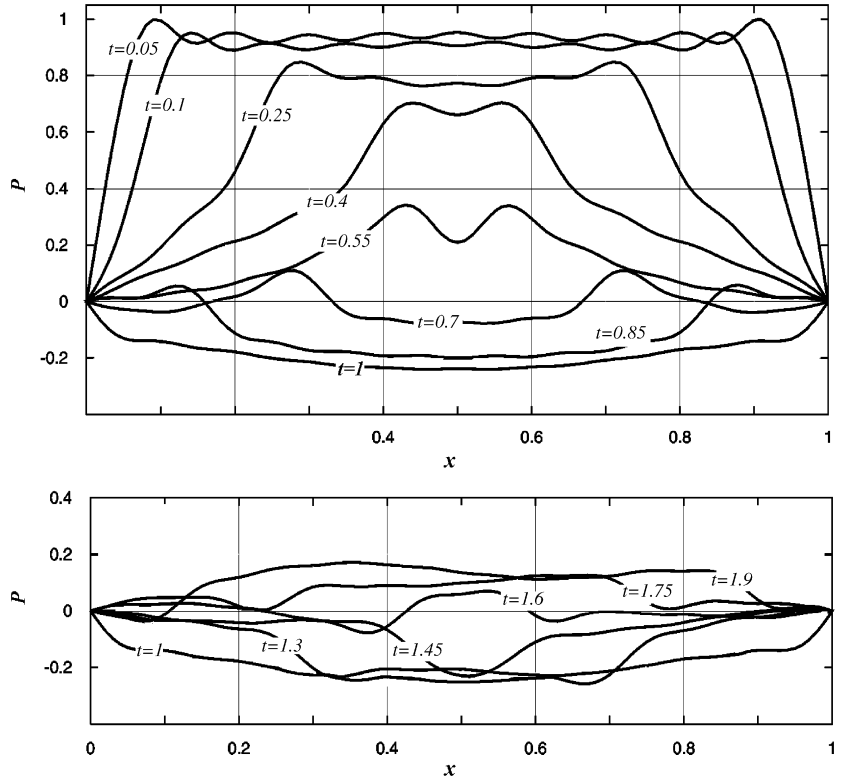

Fig. 8. Evolution of the pressure distribution along the jet cross-section in nondimensional form.

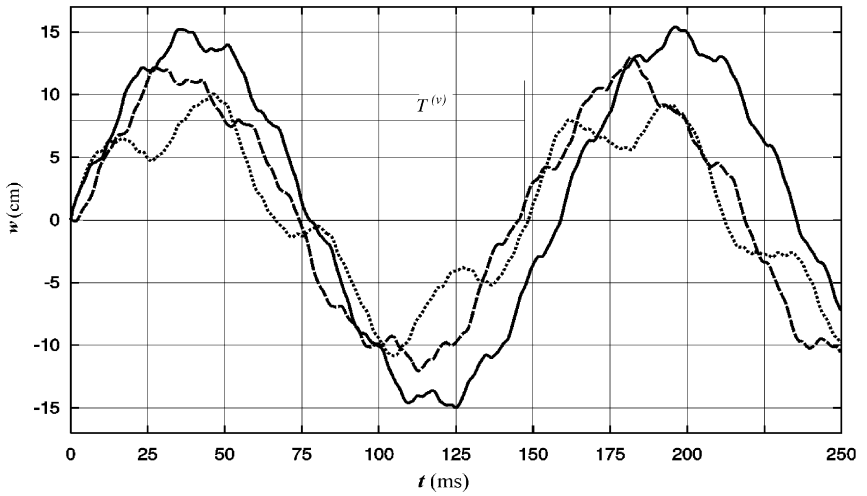

Fig. 9. Plate deflections at the plate centre in the case of symmetrical impact ($\tilde{c}=2$ m, $x=2$ m, solid line). Dotted line is for centre of the plate ($x=2$ m) and dashed line is for the centre of the jet ($x=1$ m) in the case of asymmetrical impact ($\tilde{c}=1$ m).

Calculations were performed also for the same plate but for jet impact at the plate centre ($\tilde{c} = 0.5\,\mathrm{m}$). In this case the main period of the plate vibration $T^{(v)}$ is about 22.6 ms. The maximal deflection $w_{\max} = 1.06\,\mathrm{cm}$ and maximal strain $\varepsilon_{\max} = 8717\,\mu\mathrm{s}$ occur at $t_{\max} = 5.33\,\mathrm{ms}$ at the plate centre. Both stresses and deflections for the centre impact problem are higher than those during off-centre impact (for the given impact conditions).

Results depicted in Fig. 9 are obtained for the plate length $\tilde{a}_p = 4\,\mathrm{m}$, plate thickness $\tilde{h} = 5\,\mathrm{cm}$, jet width $\tilde{a}_j = 1\,\mathrm{m}$ and impact velocity $V = 25\,\mathrm{m/s}$. The number of modes are $N_p = 20$ for the plate and $N_j = 10$ for the jet. The dimensionless time step is $\Delta t = 0.01$, which corresponds to $6.7 \times 10^{-6}\,\mathrm{s}$. Two cases are considered: centre impact with $\tilde{c} = 2\,\mathrm{m}$ and off-centre impact with $\tilde{c} = 1\,\mathrm{m}$. In the first case we found that the maximal deflection occurs at the centre of the plate, which is shown by the solid line in the figure. In the case of off-centre impact the maximal deflection occurs away from both the centre of the plate or the jet centre. The maximum of the plate deflection is equal to 12.9 cm, which occurs at $t_{\max} = 28\,\mathrm{ms}$. The maximal deflection at the centre, on the other hand, is equal to 12.5 cm at $t_{\max} = 27.2\,\mathrm{ms}$. In both cases $T^{(v)} \approx 145\,\mathrm{ms}$, while the free vibration period $T_1^{(f)} = 130\,\mathrm{ms}$. We may conclude that location of the jet impact has little effect on the period of the plate vibration during compressible jet impact onto an elastic plate.

Comparing the bending stresses obtained in the problems of centre and off-centre impacts, we find that in the off-centre impact problem the stresses are higher than in the problem of centre impact, despite the fact that the maximal deflection is smaller in the off-centre impact case.

In the centre impact case, the maximal strain of $\varepsilon_{\max} = 8157\,\mu\mathrm{s}$ occurs at the centre of the plate at $t_{\max} = 34.5\,\mathrm{ms}$, while in the off-centre impact case $\varepsilon_{\max} = 12\,417\,\mu\mathrm{s}$ occurs near the plate centre, $x_{\max} = 2.3\,\mathrm{m}$, and much earlier: $t_{\max} = 27\,\mathrm{ms}$. This observation indicates that the contribution of the higher elastic modes is much more pronounced in the off-centre impact case.

7. Three-dimensional problem of jet impact onto a rectangular plate

Impact of a compressible jet with a rectangular cross-section onto an elastic rectangular plate is considered. A sketch of this impact problem is depicted in Fig. 10. The impact region is shown in the shaded area. The width of the jet cross-section in the x-direction is taken as the length scale R. Then a_p and b_p are the nondimensional width and length of the plate respectively, b_j is the length of the jet cross-section in the y-direction and (x_c, y_c) are the coordinates of the jet centre. The jet cross-section D corresponds to the rectangular region $(x_c - \frac{1}{2}, x_c + \frac{1}{2}) \times (y_c - b_j/2, y_c + b_j/2)$.

Eqs. (1)–(5) for the hydrodynamic part of the impact problem retain their forms. The eigenfunctions $A_{nl}(x, y)$ and the eigenvalues λ_{nl} are

$$A_{nl} = \frac{2}{\sqrt{b_j}} \sin\left[\lambda_x^{(n)}\left(x - \left(x_c - \frac{1}{2}\right)\right)\right] \sin\left[\lambda_y^{(l)}\left(y - \left(y_c - \frac{b_j}{2}\right)\right)\right],$$

$$\lambda_x^{(n)} = \pi n, \quad \lambda_y^{(l)} = \frac{\pi l}{b_j},$$

$$\lambda_{nl} = \sqrt{(\lambda_x^{(n)})^2 + (\lambda_y^{(l)})^2} = \pi\sqrt{n^2 + l^2/b_j^2}. \tag{37}$$

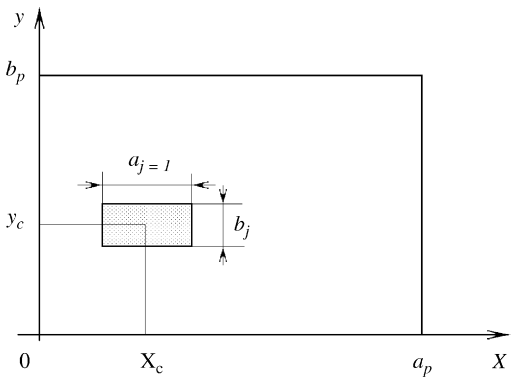

Fig. 10. Sketch of the three-dimensional impact problem.

Eq. (14) gives

$$c_{nl} = \frac{2\sqrt{b_j}}{\pi^2 nl}[1-(-1)^n][1-(-1)^l].$$

For the rectangular elastic plate $S = (0, a_p) \times (0, b_p)$ Eq. (22) can be written as

$$\Delta^2 \psi_{pq} = \kappa_{pq}^4 \psi_{pq} \quad ((x, y) \in S).$$

The boundary conditions for a simply supported plate are

$$\psi_{pq} = 0, \quad \Delta\psi_{pq} = 0 \quad ((x, y) \in \partial S).$$

The eigenfunctions $\psi_{pq}(x, y)$ are

$$\psi_{pq}(x, y) = \frac{2}{\sqrt{a_p b_p}} \sin[\kappa_x^{(p)}\, x] \sin[\kappa_y^{(q)}\, y],$$

$$\kappa_x^{(p)} = \frac{\pi p}{a_p}, \quad \kappa_y^{(q)} = \frac{\pi q}{b_p}, \quad \kappa_{pq} = \pi\sqrt{p^2/a_p^2 + q^2/b_p^2}.$$

The integrals in Eq. (25) are calculated analytically. We find

$$T_{nl,pq} = \int_{x_c-1/2}^{x_c+1/2} \int_{y_c-b_j/2}^{y_c+b_j/2} A_{nl}(x, y)\psi_{pq}(x, y)\, \mathrm{d}x\, \mathrm{d}y = \sqrt{\frac{b_j}{a_p b_p}} \left\{ \frac{\sin[\alpha_-(1)]}{\alpha_-(1)} \cos[\alpha_-(2x_c)] - \frac{\sin[\alpha_+(1)]}{\alpha_+(1)} \cos[\alpha_+(2x_c)] \right\}$$
$$\times \left\{ \frac{\sin[\beta_-(b_j)]}{\beta_-(b_j)} \cos[\beta_-(2y_c)] - \frac{\sin[\beta_+(b_j)]}{\beta_+(b_j)} \cos[\beta_+(2y_c)] \right\},$$

where

$$\alpha_-(x) = \frac{\pi}{2}\left(n - p\frac{x}{a_p}\right), \quad \alpha_+(x) = \frac{\pi}{2}\left(n + p\frac{x}{a_p}\right),$$

$$\beta_-(x) = \frac{\pi}{2}\left(l - q\frac{x}{b_p}\right), \quad \beta_+(x) = \frac{\pi}{2}\left(l + q\frac{x}{b_p}\right).$$

The periods of free vibration of the rectangular plate are given by the formulae [see Timoshenko (1955)]

$$T_{p,q}^{(f)} = \frac{2\pi}{\kappa_{pq}^2}\sqrt{\frac{\rho_p h}{D_p}}.$$

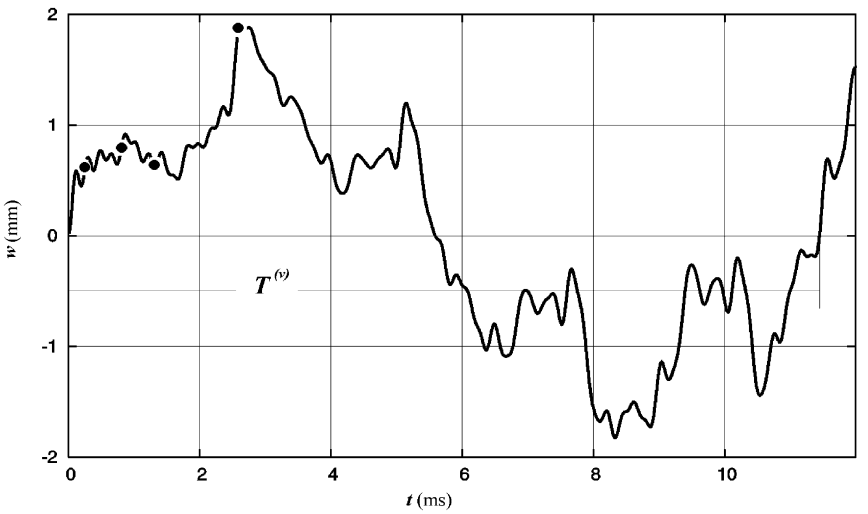

Fig. 11. Time history of the deflection at the plate centre.

The three-dimensional jet impact problem is solved numerically using the same procedure as that described in Section 5 for the two-dimensional impact problem. In order to do this, the eigenvalues λ_{nl}, κ_{pq} and the corresponding eigenfunctions are arranged in a special way. We evaluate the eigenvalues λ_{nl} of the jet cross-section by Eq. (37) and arrange them with index $k = k(n,l)$, $k = 1,2,3\ldots$ in such a way that if $k_1 < k_2$, then $\lambda_{k_1} \leqslant \lambda_{k_2}$. This means that the eigenfunctions with smaller eigenvalues enter the analysis before the eigenfunctions with higher eigenvalues. The same procedure is applied to the eigenvalues of plate vibration κ_m, where $m = m(p,q)$. We get $\kappa_{m_1} \leqslant \kappa_{m_2}$, if $m_1 < m_2$. It should be noted that the orthogonality conditions given by Eqs. (10) and (23) and all other formulae in Sections 3 and 4 are valid with $k = k(n,l)$ and $m = m(p,q)$.

Results depicted in Figs. 9–11 are obtained for a steel plate. The dimensions of the plate are 1 m × 1 m, the plate thickness is 2 cm, the jet cross-section is 20 cm × 20 cm and the centre of the jet coincides with the centre of the plate. The impact velocity is $V = 25\,\mathrm{m/s}$. The dimensionless time step is $\Delta t = 0.04$, which corresponds to 5.3×10^{-6} s. Calculations were performed with 100 modes for the plate and 100 modes for the jet, which was found to be sufficient to provide converged results [see Korobkin et al. (2006)].

Fig. 11 presents the deflection at the centre of the plate as a function of time. As in the case of a two-dimensional impact problem, the plate deflection in Fig. 11 is not entirely periodic, which is due to the memory effect. Rough estimation of the main period $T^{(v)}$ of the plate vibration due to the impact gives $T^{(v)} \approx 11.4$ ms, while

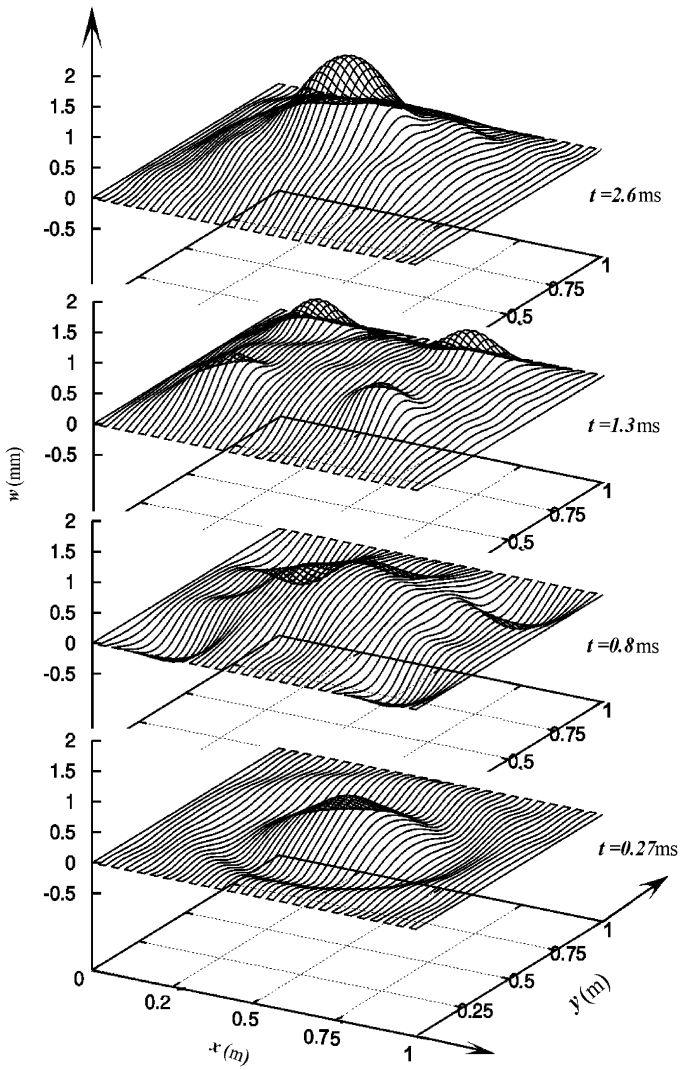

Fig. 12. Evolution of the deflection over the plate 1 m × 1 m × 2 cm, centre-impact problem.

$T^{(f)}_{1,1} \approx 10.2$ ms for free vibration of this steel plate. The dots on the line correspond to the time instants in Fig. 12 when the distributions of the plate deflections are shown.

Fig. 12 presents the evolution of the plate deflection through several snapshots. At the early stage of the impact, $t = 0.27$ ms, the maximal deflection occurs at the centre of the plate. Graphically, the plate deflection appears to be somewhat axisymmetric, despite the rectangular shapes of both the plate and the jet cross-section. Within the jet, the deflection is positive (the plate is deflected in the direction of the jet flow) but outside the jet it is negative (towards the jet). At $t = 0.8$ ms most of the plate deflection is positive apart from near the plate corners. At $t = 1.3$ ms the calculations show that the plate deflection reaches its maxima near the corners. At the point (0.24, 0.24 m) and three corresponding points near the other corners the deflection is equal to 0.94 mm, while at the plate centre the deflection is 0.64 mm. Contribution from the mode $p = 3$ and $q = 3$ is clearly visible. At $t = 2.6$ ms, which is about a quarter of the period $T^{(v)}$, the deflections are positive everywhere and reach their absolute maximum at the plate centre.

Fig. 13 shows the distributions of the bending moments per unit distance M_{xx} and M_{xy} over the plate, which are calculated by using the formulae

$$M_{xx} = -D_p\left(\frac{\partial^2 w}{\partial x^2} + \nu\frac{\partial^2 w}{\partial y^2}\right), \quad M_{xy} = -D_p(1-\nu)\frac{\partial^2 w}{\partial x\,\partial y}.$$

It can be seen that these distributions are highly oscillatory. The values of M_{xx} are about three times higher than those of M_{xy}. This ratio was found to be approximately constant during the calculations.

Figs. 14 and 15 show the results of calculations for off-centre impact on a steel plate of 1 m × 2 m. The plate thickness is 2 cm and the jet cross-section is 20 cm × 20 cm. The centre of the jet is located at (30, 40 cm). Calculations are performed for the impact velocity $V = 25$ m/s with nondimensional time step $\Delta t = 0.05$ which corresponds to 6.7×10^{-6} s. The number of modes is $N_p = 100$ for the plate and $N_j = 100$ for the jet.

Fig. 14 shows the plate deflection at several time instants. It was observed that the deflection maximum occurs at $t = 7$ ms and is located outside of the impact region. Fig. 15(a) shows the time history of the deflection at the plate and jet centres, and Figs. 15(b) and (c) provide the time histories of M_{xx} and M_{xy}, respectively, at the same locations. The higher frequency modes are more important for the bending moments than for the deflection. The maximal value of M_{xx} estimated by using the two curves in Fig. 15(b) is around 15 782 N and occurs at $t \approx 0.13$ ms. After this peak, the value of M_{xx} is always below 8000 N. The maximal value of M_{xy} on the other hand is less than 2000 N.

It is also interesting to note that the maximal values of w, M_{xx} and M_{xy} do not occur at the same location. For example, at $t = 7$ ms (see Fig. 14) the maximal deflection $w = 1.6$ mm occurs at the point (0.34, 1.64 m), the maximal bending moment $M_{xx} = 16\,374$ N at (0.32, 1.68 m) and the maximal bending moment $M_{xy} = 4256$ N at the point (0.18, 1.8 m). The absolute maxima of the quantities w, M_{xx} and M_{xy} do not occur simultaneously. This implies that the contributions of the higher elastic modes are strongly pronounced in the three-dimensional configuration.

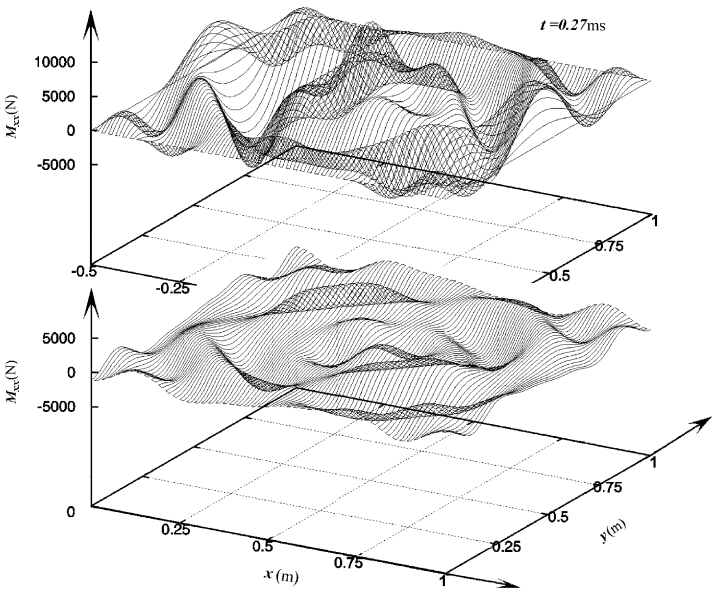

Fig. 13. Distribution of the bending moments per unit distance along x over the plate 1 m × 1 m × 2 cm, centre-impact, $t = 0.27$ ms.

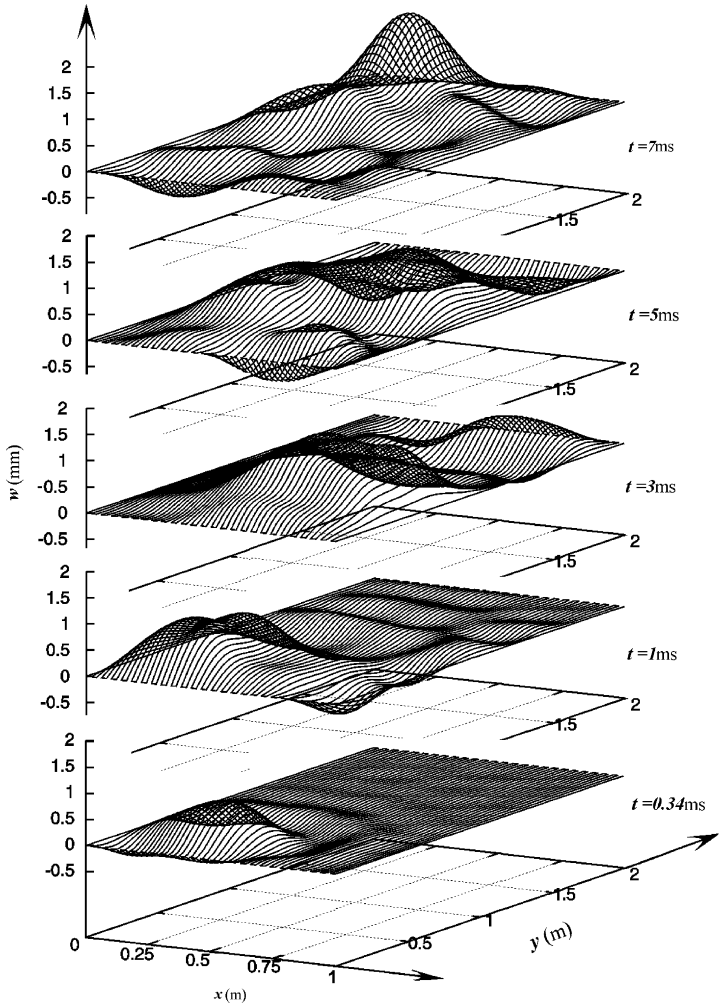

Fig. 14. Evolution of the deflection over the plate 1 m × 2 m × 2 cm, asymmetric impact.

8. Axisymmetric problem of jet impact

In the axisymmetric problem of jet impact the jet radius $\tilde{R}_j$ is taken as the length scale. The sketch of the problem in nondimensional variables is presented in Fig. 16. Eqs. (1)–(3) have the form

$$\frac{\partial^2\varphi}{\partial t^2}=\frac{\partial^2\varphi}{\partial r^2}+\frac{1}{r}\frac{\partial\varphi}{\partial r}+\frac{\partial^2\varphi}{\partial z^2}\quad (r<1, z<0),$$

$$\varphi=0\quad (r=1, z<0),$$

$$\varphi_z=1-w_t(r,t)\quad (r\leqslant 1, z=0).$$

Eqs. (9) for the eigenfunctions become

$$\frac{\partial^2 A_k}{\partial r^2}+\frac{1}{r}\frac{\partial A_k}{\partial r}+\lambda_k^2 A_k=0\quad (r<1),$$

$$A_k=0\quad (r=1),$$

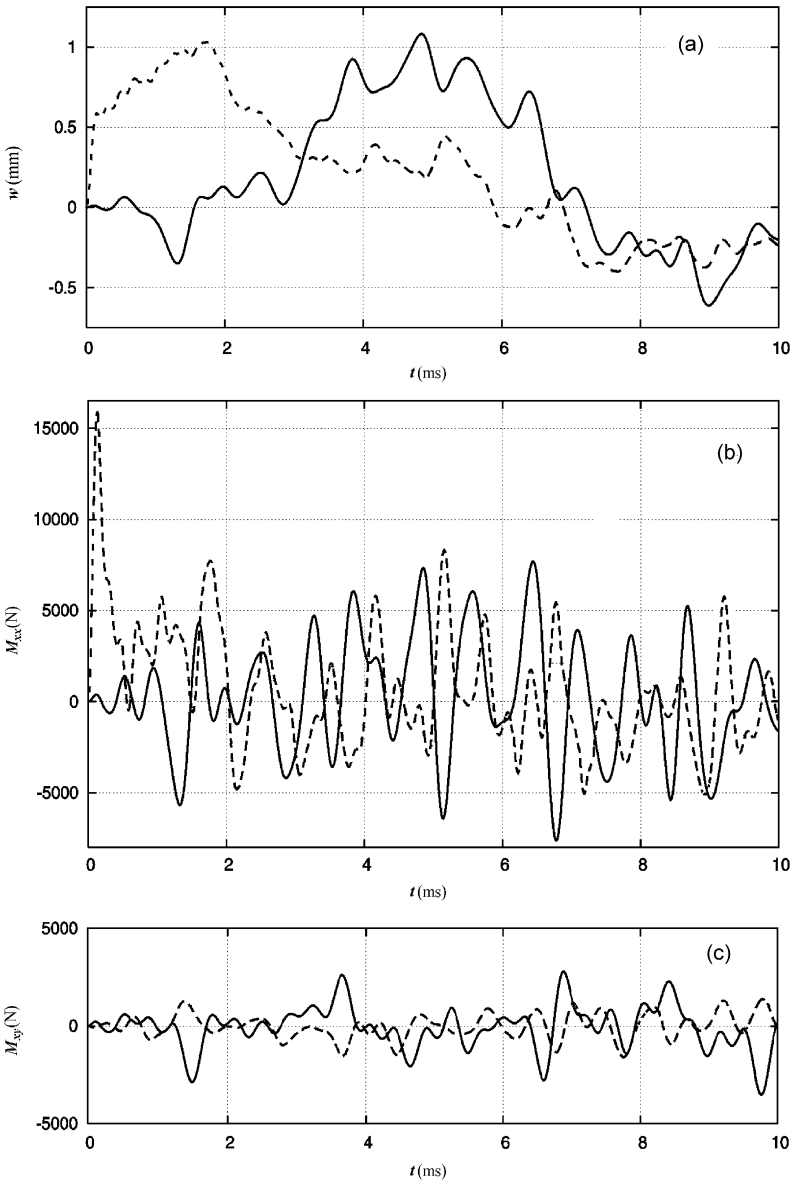

Fig. 15. Time history of the plate deflection w (a), the bending moments M_{xx} (b) and M_{xy} (c) at the plate centre (solid line) and at the jet centre (dashed line). Plate 1 m × 2 m × 2 cm, asymmetric impact with the jet centre at (0.3, 0.4 m).

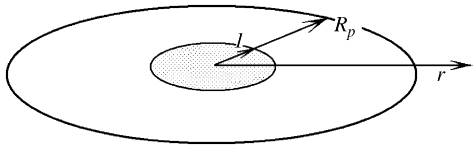

Fig. 16. Sketch of the axisymmetric impact problem.

which gives

$$A_k(r) = a_k \mathrm{J}_0(\lambda_k r).$$

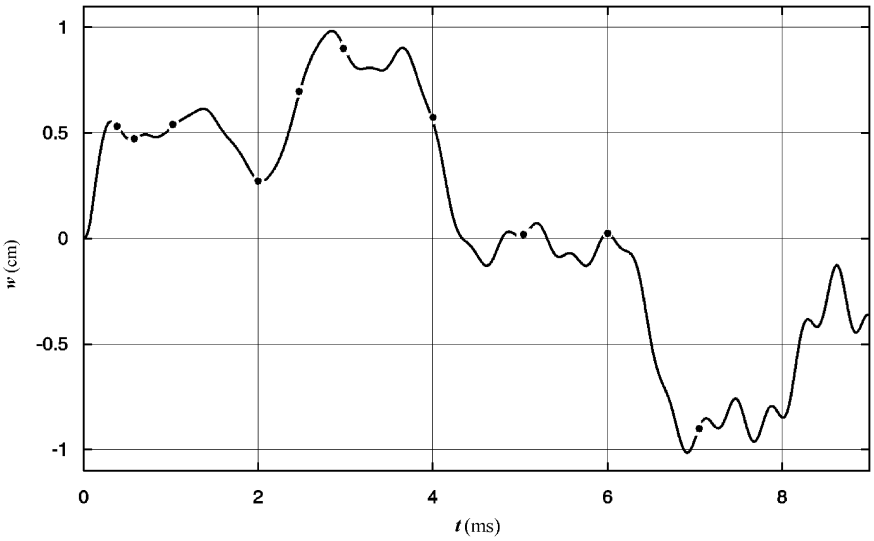

Fig. 17. Time history of the plate deflection at the centre of circular plate.

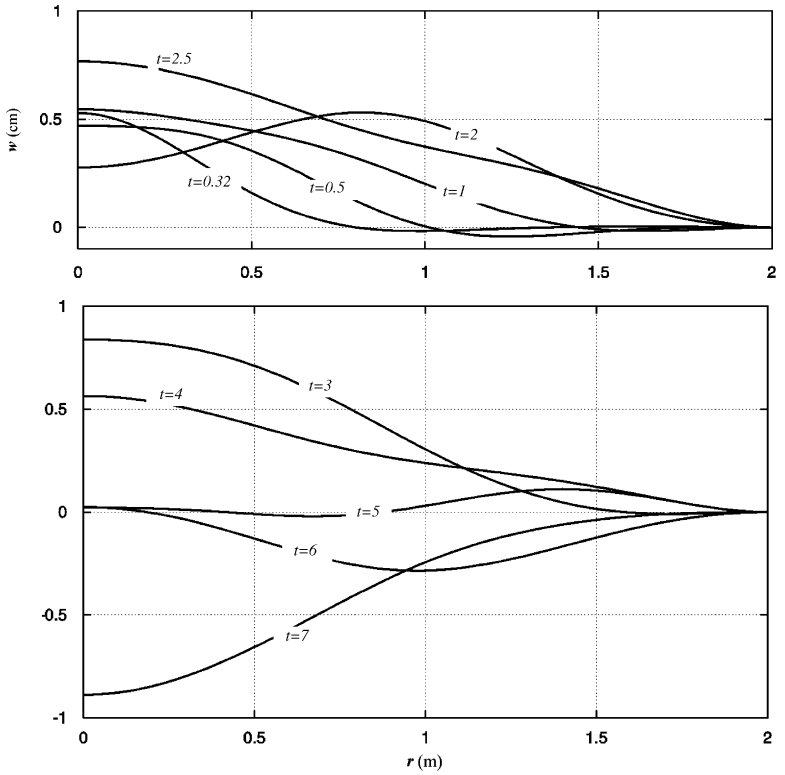

Fig. 18. Evolution of the plate deflection along the radius (time t is in microseconds).

The coefficients a_k, $k \geqslant 1$, are calculated by using Eq. (10)

$$a_k = \pi^{-1/2} \mathrm{J}_1^{-1}(\lambda_k),$$

where λ_k are zeros of the Bessel function $J_0(r)$. From Eq. (14), c_k are obtained as

$$c_k = 2\pi \int_0^1 A_k(r) r \, dr = \frac{2\sqrt{\pi}}{\lambda_k}.$$

The normal modes of the circular plate satisfy the equation

$$\left(\frac{\partial^2}{\partial r^2} + \frac{1}{r}\frac{\partial}{\partial r}\right)^2 \psi_m = \kappa_m^4 \psi_m \quad (r < R_p).$$

We consider the case of a clamped plate for which the boundary conditions are

$$\psi_m = 0, \quad \frac{d\psi_m}{dr} = 0 \quad (r = R_p).$$

We obtain

$$\psi_m(r) = D_m[J_0(\kappa_m r/R_p) - B_m I_0(\kappa_m r/R_p)],$$

where

$$B_m = \frac{J_0(\kappa_m)}{I_0(\kappa_m)}, \quad D_m = \pi^{-1/2} R_p^{-1} [2J_0^2(\kappa_m) + J_1^2(\kappa_m) - B_m^2 I_1^2(\kappa_m)]^{-1},$$

$I_0(x)$ and $I_1(x)$ are the modified Bessel functions of zero and first order, respectively. The eigenvalues κ_m are the positive roots of the equation

$$J_1(\kappa_m) I_0(\kappa_m) + J_0(\kappa_m) I_1(\kappa_m) = 0.$$

The integrals T_{km} in Eq. (25) are calculated as

$$T_{km} = 2\pi \int_0^1 A_k(r) \psi_m(r) r \, dr = -2\pi a_k D_m R_p^2 \lambda_k J_1(\lambda_k) \left[\frac{J_0(\kappa_m/R_p)}{\kappa_m^2 - R_p^2 \lambda_k^2} + B_m \frac{I_0(\kappa_m/R_p)}{\kappa_m^2 + R_p^2 \lambda_k^2}\right].$$

Figs. 17 and 18 present results for a steel circular plate with radius $\tilde{R}_p = 2\,\text{m}$ and thickness $\tilde{h} = 1.5\,\text{cm}$, which is subject to impact by a jet of radius $\tilde{R}_j = 0.5\,\text{m}$. The impact velocity is $25\,\text{m/s}$. In the calculations $N_p = N_j = 10$ and the dimensionless time step $\Delta t = 0.02$ which corresponds to $6.7 \times 10^{-6}\,\text{s}$.

Fig. 17 depicts the deflection at the centre of the plate as a function of time. The dots in Fig. 17 are time instants for which the distributions of the plate deflection along the radius are given in Fig. 18. The unit of the time in Fig. 18 is microsecond.

9. Conclusion

The coupled problem of compressible jet impact onto elastic plates has been investigated. The initial stage of the liquid–plate interaction was the main concern in this paper. This is the stage during which hydrodynamic loads, deflection and stresses may take their maximal values. The duration of the initial stage is of the order of milliseconds, which makes it possible to neglect temporal variation of the impact region and to linearize the equations of motion and the boundary conditions. On the other hand, the interaction between the compressible jet and elastic plate is strong. The problem was treated as a linear hydroelastic problem. By using the normal mode method and the Laplace transform, the problem was reduced to a system of ordinary differential and integral equations in time with respect to the principal coordinates of the velocity potential and the plate deflection. "Memory" effects were taken into account. The system has been truncated and solved numerically by the fourth-order Runge–Kutta method and the integral terms were computed by the trapezoidal rule. Three important cases have been considered, which include a two-dimensional problem of jet impact onto a simply supported beam, an axisymmetric problem of circular jet impact onto a clamped circular plate and a three-dimensional problem of rectangular jet impact onto a simply supported rectangular plate. Both the plate deflection and the stress distribution over the plate were computed and analysed in each problem.

It was shown that convergent results can be obtained with 10 modes in two-dimensional and axisymmetric problems. In the three-dimensional problem more modes must be used in the numerical calculations. The more elastic modes in the calculations, the smaller the time step Δt should be in the numerical integration of the system of Eqs. (29)–(32). Correspondingly, to achieve better accuracy, more computational time should be spent for evaluation of the integral terms in Eq. (31).

The results obtained show that the plate responds to the jet impact by vibration. The vibration does not show a strong periodic character, but the effect of the first modes is evident. The periods of vibration of these modes are longer than those of free vibrations, which is due to the "added mass" effect. The location of the impact region seems to have little effect on the period of the plate vibration.

Acknowledgements

The authors are most grateful to the Royal Society of London (International Joint Project 2005-R2) for its support to carry out this joint research. The work was also supported by the Russian Academy of Sciences (Grant no. 4.14.3) and by a grant of the President of the Russian Federation for the Leading Scientific Schools (Nsh-2260.2008.1). The authors would like to thank Dr Mark Blyth at the School of Mathematics, University of East Anglia for his valuable discussions.

References

Bredmose, H., Peregrine, D.H., Thais, L., 2002. Violent sloshing. In: Proceedings of the 17th International Workshop on Water Waves and Floating Bodies, Cambridge, UK, pp. 13–16.

Eroshin, V.A., Pomanenkov, N.I., Serebrjakov, I.V., Yakimov, Y.L., 1980. Hydrodynamic forces at blunt body impact on a compressible fluid surface. Izvestiya Akadademii Nauk SSSR, Mekhanika Zidkosti i Gaza 6, 44–51.

King, A.C., Needham, D.J., 1994. The initial development of a jet caused by fluid, body and free-surface interaction. Part 1. A uniformly accelerated plate. Journal of Fluid Mechanics 268, 89–101.

Korobkin, A.A., 1996. Global characteristics of jet impact. Journal of Fluid Mechanics 307, 63–84.

Korobkin, A.A., 1998. Wave impact on the center of an Euler beam. Journal of Applied Mechanics and Technical Physics 39, 770–781.

Korobkin, A.A., Khabakhpasheva, T.I., 2006. Regular wave impact onto an elastic pate. Journal of Engineering Mathematics 55, 127–150.

Korobkin, A.A., Khabakhpasheva, T.I., Wu, G.X., 2006. Compressible jet impact onto elastic panels. In: Proceedings of the Fourth International Conference on Hydroelasticity in Marine Technology Wuxi, China, pp. 159–168.

Lu, C.H., He, Y.S., Wu, G.X., 2000. Coupled analysis of nonlinear interaction between fluid and structure during impact. Journal of Fluids and Structures 14, 127–146.

Needham, D.J., Billingham, J., King, A.C., 2007. The initial development of a jet caused by fluid, body and free-surface interaction. Part 2. An impulsively moved plate. Journal of Fluid Mechanics 578, 67–84.

Peregrine, D.H., 1972. Flow due to vertical plate moving in a channel. Unpublished notes, Department of Mathematics, University of Bristol, UK.

Timoshenko, S., 1955. Vibration Problems in Engineering. D.van Nostrand Company, New York.

Wu, G.X., 1991. Hydrodynamic impact of the water waves. In: Proceedings of the Sixth International Workshop on Water Waves and Floating Bodies, Wood Hole, MA, USA, pp. 259–263.

Wu, G.X., 2001. Initial pressure distribution due to jet impact on a rigid body. Journal of Fluids and Structures 15, 365–370.